Title: A Novel Approach to Three-Dimensional Change Detection in Multitemporal LiDAR Data Acquired in Forest Areas

This paper appears in: IEEE Transactions on Geoscience and Remote Sensing

Date of Publication: 2018

Author(s): Daniele Marinelli, Claudia Paris, Lorenzo Bruzzone

Volume:

Page(s):

DOI: 10.1109/TGRS.2018.2789660

A Novel Approach to Three-Dimensional Change Detection in Multitemporal LiDAR Data Acquired in Forest Areas

Daniele Marinelli, *Student Member, IEEE,* Claudia Paris, *Member, IEEE,*
Lorenzo Bruzzone, *Fellow, IEEE*

***Abstract*—LiDAR data have been widely used to characterize the three-dimensional structure of the forest. However, their use in a multitemporal framework has been quite limited due to the relevant challenges introduced by the comparison of pairs of point clouds. Because of the irregular sampling of the laser scanner and the complex structure of forest areas, it is not possible to perform a point-to-point comparison between the two data. To overcome these challenges, a novel hierarchical approach to the detection of 3-D changes in forest areas is proposed. The method first detects the large changes (e.g., cut trees) by comparing the Canopy Height Models (CHMs) derived from the two LiDAR data. Then, according to an object-based Change Detection (CD) approach, it identifies the single-tree changes by monitoring both the tree-top and the crown volume growth. The proposed approach can compare LiDAR data with significantly different pulse densities, thus allowing the use of many data available in real applications. Experimental results pointed out that the method can accurately detect large changes, exhibiting a low rate of false and missed alarms. Moreover, it can detect changes in terms of single-tree growth which are consistent with the expected growth rates of the considered areas.**

***Index Terms*—3-D change detection, multitemporal analysis, Light Detection and Ranging (LiDAR), remote sensing, forestry.**

I. Introduction

Forests are a living ecosystem characterized by natural and anthropogenic processes and thus they are constantly changing. Hence, it is very important to develop techniques for monitoring forest areas in order to update forest inventories (for management and planning) and to analyze the health of wooded areas (e.g., reduced growth rate due to tree diseases). Remote sensing data acquired at different times over large forest areas are a suitable information source to perform automatic CD.

In the literature, the use of remote sensing data for CD in forest areas has been addressed mainly considering multitemporal optical images. Given two images acquired on the same areas at different times, two basic approaches are usually considered: i) pixel-based analysis; ii) context-based analysis. In the first approach, a pixel-by-pixel comparison of the images is carried out by working directly on the original spectral channels or by comparing features extracted from them (e.g., Normalized Difference Vegetation Indices) [1]. However, this approach does not exploit the contextual information of the neighbouring pixels. In contrast, the context-based approach uses the local spatial information to better characterize the objects in the multitemporal analysis (e.g., comparison of all the pixel belonging to a tree crown). It is worth noting that, for an accurate CD, the group of pixels associated with a given object should be chosen accurately either by using GIS data [2] or by applying a segmentation method to the images in order to identify uniform areas [3]. Both approaches (pixel-based and context-based) can be applied to bi-temporal images or to time series of images [4] to evaluate the vegetation variation trend during the year. In CD applied to forestry, it is important to identify the changes by discriminating between different types of variations. When dealing with multispectral or hyperspectral images, multiple spectral bands can be used to discriminate among different changes. In [5] the authors propose an unsupervised approach to CD based on the polar Change Vector Analysis (CVA). By using this polar CVA representation, it is possible to better distinguish between the different types of changes exploiting the spectral information present in the data. More in general, there are many techniques presented in the literature that can effectively solve the CD problem in forest areas by using optical data. However, multispectral and hyperspectral data do not contain any information for characterizing the three-dimensional structure of a forest. Accordingly, they are not suitable for a detailed analysis of the 3-D geometrical changes of the trees (e.g., changes in volume and height). Moreover, optical data are very sensitive to the period and the acquisition conditions. According to the season in which the data are acquired, the spectral response of the tree crowns may significantly change thus leading to false alarms. Furthermore, different illumination conditions may affect the CD results.

In contrast, Light Detection and Ranging (LiDAR) data accurately measure the 3-D structure of the analyzed scene, thus collecting valuable informations for forestry applications. Moreover, LiDAR is not affected by illumination conditions, even though the acquisition season may affect the acquired data due to the variation of the foliage in the case of broadleaf (i.e., leaf-on or leaf-off conditions). LiDAR data have been widely employed for the estimation of forest parameters on single acquisitions. Nonetheless, only few papers addressed the challenging problem of the analysis of multitemporal LiDAR data for 3-D CD. In particular, three main problems should be considered: i) the pulse density of the two point clouds can be significantly different; ii) the irregular sampling of the LiDAR pulses results in measures that are not uniformly distributed; iii) the tree crowns are characterized by an irregular structure. For all these reasons, the probability that the LiDAR pulses

hit the same portion of the crown in two different acquisitions is very small.

A possible solution to these problems is to perform the comparison by estimating forest attributes at stand level. Instead of directly comparing the point clouds, the multitemporal analysis is performed on the parameters estimated from the LiDAR data at plot level. In [6]–[8] the authors perform CD by estimating the Above Ground Biomass (AGB) variation. In [6] the AGB changes are estimated following two approaches. In the first one they analyze the variation of LiDAR height metrics and relate them with biomass variation, while in the second they compare the AGB estimates obtained at the two dates. The first approach proved to be accurate at a scale of $10\,ha$, whereas the second one showed good results at $1\,ha$ scale. In [7], the authors independently estimate the AGB at the two considered dates and then analyze their difference in order to quantify the AGB variation in areas affected by logging. In [9], the authors estimated the Leaf Area Index (LAI) and subsequently computed the LAI variation as the difference of the estimates to analyze the effects of an insect attack on Scots pines. However, all these stand level approaches work at large scale ($50\,m$ [7], $10\,m$ [9]) or at coarse scales ($0.25-10\,ha$ [6], [8]). Thus, they are not suitable for an individual tree level analysis. In addition, they require field measurements for relating the LiDAR point clouds with the forest parameters that have to be estimated, which are not always available.

In [10]–[14] the authors use multitemporal LiDAR datasets to search for canopy gaps opening or closing. A common approach is to detect the canopy gaps by computing the difference between the two Canopy Height Models (CHM) [10]–[12], which are the regularized version of the LiDAR data on 2-D grids (i.e., image domain). The regularization step simplifies the CD analysis since it mitigates the effect of the non uniform laser sampling and the irregular structure of the crown. In [10]–[12] the difference image is thresholded in order to obtain a binary map. In other papers, the authors first detect the canopy gaps in the CHMs separately at the two dates and then compare the obtained sets in order to identify canopy gaps opening or closing [13], [14]. To remove noise (i.e., small patches of pixels wrongly identified as canopy gaps), various methods have been proposed, such as the removal of all the patches with area smaller than a given threshold [10], [12], [14] or the elimination of the areas where the corresponding pixels of the CHM contain few laser pulses [10], [14]. All these methods are suitable for the analysis of canopy gaps and their dynamics, which are large changes that do not require any detailed analysis.

In order to detect changes in terms of height and volume growth at the individual tree level, specific techniques should be used. First, the individual trees have to be identified and segmented. Many methods have been presented in the literature to perform the segmentation both in the CHM and point cloud domains [15]–[19]. A typical approach is the search for the maxima in the CHM which are then used as seeds in a region growing approach [15]. In [16] the authors perform the segmentation by working both in the regularized domain of the CHM (to delineate the crowns) and in the point cloud domain (to distinguish between understory and overstory vegetation). In [17] the point cloud is seen as a 3-D multimodal distribution where each mode represents a possible tree crown. A mean-shift algorithm is used to identify the considered modes. Other methods are based on a directional analysis of the crown profile in the point cloud domain [18] and in the regularized domain [19].

When the individual trees have been detected and segmented, the CD analysis can be performed at single-tree level [10], [11], [20]–[24]. In [11], [21], the vertical growth of a tree is computed as the difference between the highest LiDAR points of the considered tree at the two dates. This estimate is computed under the hypothesis that there is at least one laser pulse that hits the tree-top at both dates. This hypothesis can be considered valid if the pulse densities of the two point clouds are relatively high (i.e., greater than $5-10\,pls/m^2$). If this condition is not satisfied, it is possible to evaluate not only the difference of the highest LiDAR points of the tree at the two dates but also the difference between the mean and median of the values of the Digital Surface Models (DSM) representing the analyzed tree [20] or the mean of the elevation of the LiDAR points belonging to the considered tree in the two data [10]. In [22] the authors analyze the relationship between canopy gaps and the growth of individual trees by comparing the growth of the individual trees on the edge of canopy gaps (i.e., with large part of the canopy not covered by other trees) with the growth of the trees surrounded by other crowns. Regarding the horizontal growth of the canopy, in [11] an estimate is computed by measuring the difference between the areas of the segmentation regions associated to the same tree at the two dates. However, the method does not exploit the rich information content of the 3-D tree crown structure present in the point cloud. In [23], [24] the change detection is performed at individual tree level in the point cloud space. In [23] the authors analyze multitemporal terrestrial LiDAR data to assess AGB changes. For each detected tree the AGB is estimated by using the two LiDAR point clouds separately. Then, the estimates are compared to identify the biomass change per tree. In [24] a method to detect tree changes in urban areas (in which typically trees do not intersect significantly) using multitemporal high density airborne LiDAR data is presented. The parameters of the tree crown are estimated separately on the two LiDAR point clouds and then compared to estimate the tree changes.

It is worth noting that regardless of the method used to perform the CD, to obtain satisfactory results the two point clouds have to be registered. The problem of 3D point cloud registration has been extensively analyzed in the literature. The Iterative Closest Point (ICP) [25] algorithm is one of the most common solutions adopted in a large variety of datasets and contexts. ICP allows a fine registration of overlapping 3D point clouds by iteratively estimating the transformation parameters. The errors are distributed among all the points of the sets to limit distortion while preserving the geometry of the entire scene [26], [27]. However, since it is an iterative descent algorithm, a good a priori alignment should be provided to reach the global minimum. Moreover, a major bottleneck is the rate of convergence. To refine the registration results and reduce the computational burden, local features can be

employed considering object-based approaches [28] or using local features [29], [30].

From this analysis of the literature, it turns out that little research regarding the analysis of multitemporal LiDAR data has been carried out. In particular, most of the techniques present in the literature perform the CD at stand level, thus producing maps representing the variation of forest metrics at plot level. Very little has been done regarding the single-tree analysis with most of the papers focusing on the vertical growth of the canopy. For all these reasons, in this paper we propose a novel approach to the detection of large changes (e.g., cut trees) and single-tree changes (i.e., vertical and crown volume growth) in multitemporal LiDAR data. The proposed approach is based on a hierarchical strategy that first detects the large changes and then identifies the changes at the individual tree level according to an object-based approach. This allows us to decompose the complex multitemporal analysis into simpler problems, thus simplifying the 3-D CD problem. While the large changes are detected in the CHM, the object-based approach focuses on the single-tree crowns directly in the point cloud domain to exploit the full information of the LiDAR data to detect the 3-D changes of the canopy. Unlike most of the literature methods, the proposed approach estimates both the vertical and horizontal growth to characterize the canopy volume growth. Moreover, we are able to perform the CD using point clouds with very different pulse densities. It is worth noting that the crown volume is an important tree parameter which has been demonstrated to be a good predictor for the estimation of the forest biomass [31], [32], for forest fire simulations [33], [34] and for Diameter Breast Height (DBH) estimation [35] (since DBH and crown volume are correlated). In [33] the authors estimate the crown volume and the foliage biomass to compute the single-tree crown density as the foliage biomass divided by the crown volume. Thus, the detection of the changes of the crown volume is really important for the monitoring of forest areas.

To assess the effectiveness of the proposed approach, experiments have been carried out on two forest areas located in the Southern Alps of the Trentino region (Italy). This work focuses on conifers which are the primary tree species in Alpine environment. We used both high density (up to $50\,pls/m^2$) and medium density (up to $10-15\,pls/m^2$) LiDAR data. Results confirmed the effectiveness of the proposed 3-D CD method.

The paper is organized as follows. Section II describes the proposed approach, by illustrating in detail all the different steps. The data used for the validation of the proposed method and the experimental results are presented and discussed in Section III. Finally, Section IV draws the conclusions and presents possible directions for future developments.

II. Proposed Hierarchical 3-D Change Detection Approach

The aim of the proposed hierarchical CD approach is to accurately detect 3-D forest changes in multitemporal LiDAR data. First, the method identifies the large changes (e.g., cut trees, new buildings) and then focuses the attention on the individual trees in order to detect the changes of the tree canopies both in term of vertical and crown volume variation. Figure 1 shows the architecture of the proposed method, which is composed of 3 main parts: i) pre-processing (to make the two point clouds comparable); ii) detection of large changes by comparing the two CHMs; iii) object-based detection of changes at the individual-tree level.

A. Problem definition

As mentioned in Section I, forests are characterized by heterogeneous changes. In order to correctly identify all of them, it is necessary to properly define the CD problem. Let us assume to have a multitemporal LiDAR dataset consisting of two point clouds $\mathcal{P}_1$ and $\mathcal{P}_2$ (each composed by a set of points $\mathbf{p}$ having coordinates x, y, z) acquired on the same forest area at different times t_1 and t_2, respectively. Let $\Omega = \{\Omega_l, \Omega_c, \omega_n\}$ be the set of all the considered classes where Ω_l is composed by the areas affected by large changes, Ω_c corresponds to the areas with forest canopy cover present at both dates and ω_n represents all the areas that are of no interest for forest change studies, i.e., areas that do not have any canopy cover. Class $\Omega_l = \{\omega_{ln}, \omega_{lp}\}$ represents the classes of changes corresponding to large negative changes ω_{ln} (e.g., cut trees, destroyed buildings) and large positive changes ω_{lp} (e.g., new trees or buildings). Finally, $\Omega_c = \{\omega_{ng}, \omega_g\}$ represents the status of the areas covered by trees. We distinguish between trees with no growth (class ω_{ng}) and trees that have changed between the two acquisitions (class ω_g). Class ω_g represents the growth of the trees both in terms of vertical variation dH and crown volume variation dV. It is worth noting that dH and dV are not mutually exclusive but they are usually correlated as the height variations contribute also to crown volume growth. Figure 2 shows the modeling of the hierarchical tree structure in the considered CD problem.

B. Pre-processing

The aim of the pre-processing is to make the two point clouds $\mathcal{P}_1$ and $\mathcal{P}_2$ comparable to accurately perform the multitemporal analysis. Accordingly, first we register the two data by applying the ICP algorithm, which aims at minimizing the Euclidean distance between the two 3-D point clouds. In this step we assume that a large portion of the forest did not change significantly between the two acquisitions. To this end, the algorithm iteratively searches for the rigid transformation $\mathcal{T} = [R|t]$ (defined by a rotation matrix R and a translation vector t) that best aligns the two LiDAR data. This is done by finding, at each iteration, a one-to-one correspondence between the points of $\mathcal{P}_1$ and the reference point cloud $\mathcal{P}_2$ thus generating a set of Q matched points $\{\mathbf{p}_{1,q}, \mathbf{p}_{2,q}\}_{q=1}^{Q}$. The algorithm searches for a transformation $\mathcal{T}$ that minimizes the Euclidean distance between each point $\mathbf{p}_{2,q}$ and the corresponding transformed point $\mathbf{p}_{1,q}^{\mathcal{T}} = R\mathbf{p}_{1,q} - t$, i.e.,:

$$d(\mathbf{p}_{1,q}^{\mathcal{T}}, \mathbf{p}_{2,q}) = ||\mathbf{p}_{1,q}^{\mathcal{T}} - \mathbf{p}_{2,q}||. \quad (1)$$

Thus, the algorithm searches for the $\mathcal{T}$ such that:

$$\mathcal{T} = \underset{\mathcal{T}'}{\operatorname{argmin}}\, \mathcal{E}(\mathcal{T}') = \underset{\mathcal{T}'}{\operatorname{argmin}} \sum_{q=1}^{Q} d(\mathbf{p}_{1,q}^{\mathcal{T}'}, \mathbf{p}_{2,q}). \quad (2)$$

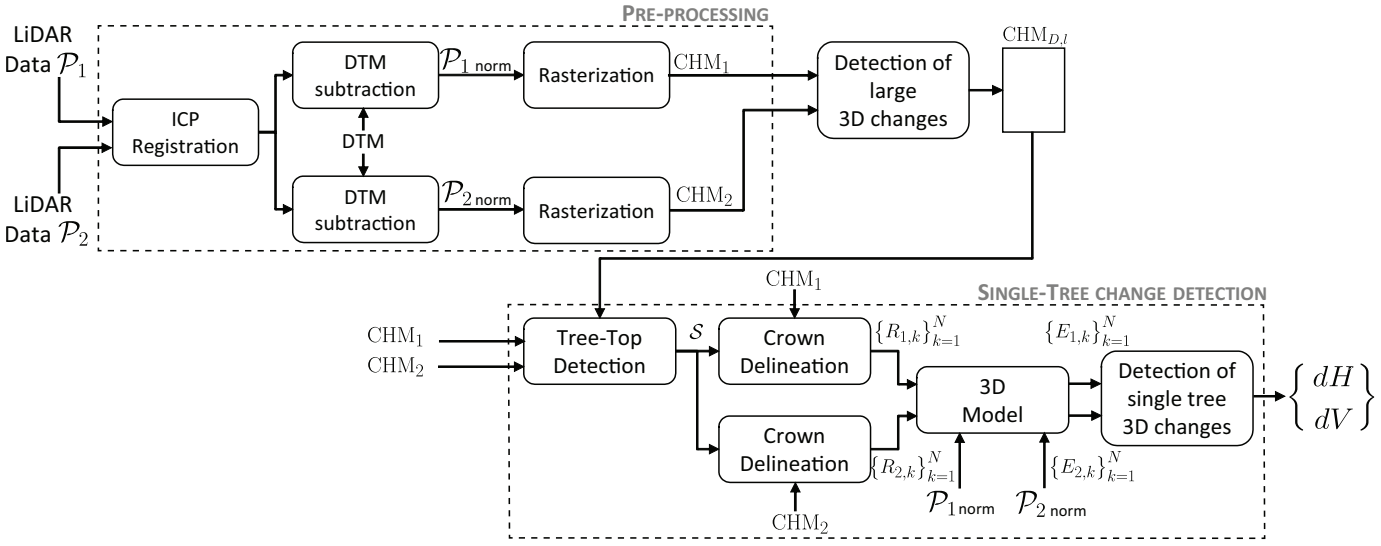

Fig. 1: Architecture of the proposed method for the detection of large changes and single-tree changes.

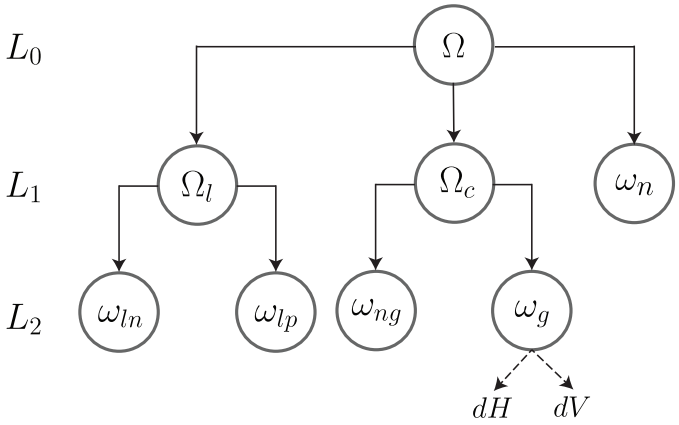

Fig. 2: Hierarchical tree structure of the considered CD problem in forest areas. The represented classes are: Ω set of all considered classes; Ω_l large changes; ω_{ln} large negative changes; ω_{lp} large positive changes; Ω_c forest canopy cover present at both dates; ω_{ng} trees with no growth; ω_g trees with growth; ω_n areas of no interest for forest change studies.

The transformation $\mathcal{T}$ is applied to the point cloud $\mathcal{P}_1$ (or $\mathcal{P}_2$ if the reference point cloud is $\mathcal{P}_1$). The algorithm then defines a new set of matched points between the reference and transformed point clouds and searches for a new transformation. These operations are repeated until $\mathcal{E}(\mathcal{T})$ is smaller than a given threshold. It is worth noting that the ICP algorithm was originally developed for computer vision applications. Thus, it has been applied mostly to 3-D models having a very high point density. Moreover, a basic assumption of the original ICP is that the two 3-D models are almost identical (at least the portions that have to be aligned). Unfortunately, this is not the case for multitemporal airborne LiDAR data acquired on forest areas. Hence, the point-to-point approach of the ICP may lead to compute the rigid transformation using unreliable pairs of points. To mitigate the effects of this problem, we use only the first return of the two point clouds, thus considering only the external surface of the tree crowns, which is also the most informative. In addition, we discard a given percentage of pairs of points with the largest Euclidean distance. In particular, at each iteration we compute the set $D = \{d(\mathbf{p}_{1,q}, \mathbf{p}_{2,q})\}_{q=1}^{Q}$ of the Euclidean distances between all the pairs of matched point (before computing the transformation) and we define a binary variable w_q as:

$$\mathsf{w}_q = \begin{cases} 0 & d(\mathbf{p}_{1,q}, \mathbf{p}_{2,q}) > P_r(D) \\ 1 & d(\mathbf{p}_{1,q}, \mathbf{p}_{2,q}) \leq P_r(D) \end{cases}, \forall q = 1, \ldots, Q, \quad (3)$$

where $P_r(D)$ is the r$^{\text{th}}$ percentile of D. The defined binary variable w_q can be used in $\mathcal{E}(\mathcal{T}')$ to discard pairs of point for which the pairwise Euclidean distance is large, i.e.,:

$$\mathcal{E}(\mathcal{T}') = \sum_{q=1}^{Q} \mathsf{w}_q d(\mathbf{p}_{1,q}^{\mathcal{T}'}, \mathbf{p}_{2,q}) \quad (4)$$

These points cannot be used to reliably compute the transformation because they have a high probability of not representing the same portion of the tree or ground at the two dates. This may be due to outliers or large changes (e.g., a point representing a branch of a tree that has been cut between the two acquisitions should not be used in the ICP). Moreover, we decimate the two point clouds in order to apply the ICP on two data with the same density. Note that the ICP is applied to the two point clouds before subtracting the Digital Terrain Model (DTM). This allows us to use the information regarding the morphology of the terrain in the registration step. The transformation is applied also to the discarded points, which are considered in all the following steps.

After the registration phase, a DTM is subtracted from the two LiDAR data to obtain the relative height of the points with respect to the ground (i.e., normalized point clouds $\mathcal{P}_1$ and $\mathcal{P}_2$). Then, we regularize the two LiDAR data on a square

grid. To this aim, we compute the value for each square as the elevation of the highest point which x, y coordinates fall inside the cell. Subsequently, to fill the gaps in the grid due to missing points, we apply an interpolation algorithm [36]. Finally, the regularized point clouds can be easily converted into images, thus obtaining the two Canopy Height Models CHM_1 and CHM_2.

C. Detection of Large Changes

According to the hierarchical approach, first we need to automatically identify the areas affected by large positive ω_{lp} and negative ω_{ln} changes. To this end, we compute the difference image CHM_D by subtracting CHM_1 and CHM_2 [10]–[12] as follows:

$$\text{CHM}_D(x,y) = \text{CHM}_2(x,y) - \text{CHM}_1(x,y). \tag{5}$$

As we are searching for large changes, to identify only the areas in which there is a substantial height variation, two thresholds $t_{h,lp}$ and $t_{h,ln}$ are applied to CHM_D, in order to obtain two binary maps $\text{CHM}_{D,lp}(x,y)$ and $\text{CHM}_{D,ln}(x,y)$ according to:

$$\begin{aligned} \text{CHM}_{D,lp}(x,y) &= \begin{cases} 1 & \text{CHM}_D(x,y) \geq t_{h,lp} \\ 0 & \text{otherwise} \end{cases} \\ \text{CHM}_{D,ln}(x,y) &= \begin{cases} 1 & \text{CHM}_D(x,y) \leq -t_{h,ln} \\ 0 & \text{otherwise} \end{cases} \end{aligned} \tag{6}$$

where the pixels set to 1 identify the areas affected by large changes (positive changes ω_{lp} for $\text{CHM}_{D,lp}(x,y)$ and negative changes ω_{ln} for $\text{CHM}_{D,ln}(x,y)$). We use two thresholds (considering $t_{h,lp} < t_{h,ln}$) since the magnitude of the deforestation changes can be much larger with respect to the one of the forestation changes. Indeed, whereas the cut of a tree may correspond to a variation of more than $30\,m$, the growth of a new tree corresponds to much lower absolute values in $\text{CHM}_D(x,y)$, which depend also on the elapsed time between the two acquisitions. It is worth noting that the choice of two different threshold values does not affect the detection of other large changes such as the construction or destruction of buildings since their magnitude is large both for positive and negative changes. Then we perform a series of morphological operations on both binary maps starting with an erosion filter based on a circular structuring element. This operation allows us to remove most of the noise, thus identifying either the cut or new tree canopies and other large changes. Then, all the regions with area lower than a given threshold t_A are removed and finally a dilation filter (having the same structuring element used in the previous morphological operation) is applied to the resulting binary image. It is worth noting that the size of the structuring element and the threshold area t_A should be chosen according to the spatial resolution of the CHMs. The obtained binary maps $\text{CHM}_{D,ln}(x,y)$ and $\text{CHM}_{D,lp}(x,y)$ are then merged in a single map $\text{CHM}_{D,l}(x,y)$ which is used to drive the detection of the single-tree changes, i.e., all the operations of the second part of the method are applied only on to the areas that are not affected by large changes. At this point of the analysis, all the areas not affected by large changes may belong to areas not of interest for forest studies (i.e., ω_n class) or to areas with the presence of canopy cover at both dates (Ω_c).

D. Single-Tree Change Detection

In the last step of the proposed hierarchical approach, we address the difficult task of detecting the single-tree changes and the related attributes dH and dV. This requires to accurately detect and delineate the tree canopies at the two dates since every error in the crown detection and delineation step will affect the single tree CD results. The individual tree crowns are detected and delineated in the CHMs and then the multitemporal analysis is performed directly in the point cloud space. This condition allows us to exploit the full information content of the point clouds to improve the detection of the single-tree changes. To overcome the problem related to the CD in multitemporal LiDAR data (i.e., point-to-point comparison is not feasible), we focus the attention on the whole tree structure by means of an object-based approach based on the geometry of the tree canopy.

To detect the trees at the two dates, first we apply median and Gaussian filtering to the two CHMs. Then, by applying a Level Set Method [35] to CHM_1 and CHM_2, we separately identify the positions of the tree-tops, hereafter referred also as seeds. This operation produces the set of seeds $\mathcal{S}_1 = \{\mathbf{s}_{1,k_1}\}_{k_1=1}^{N_1}$ at time t_1 and the set of seeds $\mathcal{S}_2 = \{\mathbf{s}_{2,k_2}\}_{k_2=1}^{N_2}$ at time t_2, where $\mathbf{s}_{1,k_1} = (x_{k_1}, y_{k_1})$ and $\mathbf{s}_{2,k_2} = (x_{k_2}, y_{k_2})$ represent the 2-D positions of the tree-tops at the two dates. According to the availability of the multitemporal dataset, we can employ in a synergistic way the two LiDAR data to improve the detection result. Thus, we compare the set of seeds $\mathcal{S}_1$ with $\mathcal{S}_2$ to match the trees present at both dates. The position of the same tree-top may be different at the two dates due to natural causes or residual registration error (which we assume to be small due to registration step applied in the pre-processing phase). Thus we can perform a final object-based registration by matching the two sets of seeds associating to each seed $\mathbf{s}_{1,k_1} \in \mathcal{S}_1$ the nearest seed $\mathbf{s}_{2,n} \in \mathcal{S}_2$ according to the Euclidean distance:

$$\mathbf{s}_{2,n} : n = \underset{k_2 \in [1,\ldots,N_2]}{\operatorname{argmin}} \|\mathbf{s}_{2,k_2} - \mathbf{s}_{1,k_1}\|. \tag{7}$$

To avoid false matching, we discard all the matched pairs having an Euclidean distance greater than a given threshold t_s. Note that the matching is performed considering only the tree-tops locations, without taking into account the tree-top heights, which change due to the vertical growth of the trees. For those seeds detected only in one acquisition, we improve the detection accuracy by using the information provided by the other acquisition. In particular, we aim to distinguish between false alarms (i.e., false tree-tops detected due to noise at one date) or true tree-tops correctly identified only at one date. To this end, we compute a rough estimate of the crown width by analyzing the behavior of the CHM around each of these seeds by means of a directional analysis. If the estimated crown width is greater than $1\,m$ at least at one of the two dates, we recover $\mathbf{s}_m$, otherwise we definitely discard it. This operation allows us to use in a synergistic way the multitemporal information to reduce the number of

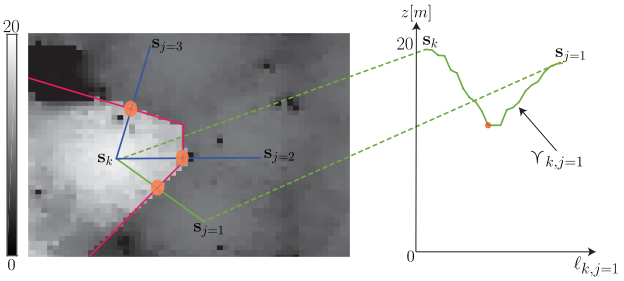

Fig. 3: Example of the first operation of the segmentation of tree $\mathbf{s}_k$ surrounded by three trees $\{\mathbf{s}_j\}_{j=1}^{3}$. In blue the lines $\ell_{k,j}$ with in green $\Upsilon_{k,j=1}$. The orange dots represent the points at which the considered tree intersects with its neighbours. The portion of the CHM shows the result of the partial segmentation as the bright area (delineated by the red bounding box).

false alarms without increasing the number of missed alarms. In this step we compute a rough estimate of the the crown radius. However, to perform an accurate CD a more precise approach to the crown delineation is required. The result of these operations is a single set $\mathcal{S} = \{\mathbf{s}_k\}_{k=1}^{N}$, where $\mathbf{s}_k = (x_k, y_k)$ represents the ground coordinates of the k^{th} tree and $N \leq \min\{N_1, N_2\}$ is the number of tree-tops detected at both dates.

To fully characterize the tree canopies, we perform the crown delineation separately in CHM_1 and CHM_2 around each $\mathbf{s}_k \in \mathcal{S}$. In the CD segmentation errors may lead to the detection of changes which are not related to the growth of the trees. Thus, we aim to perform a conservative segmentation to reduce the number of errors (i.e., portions of crowns that are included in the segmentation region of other tree canopies). For this reason, in the first phase of the segmentation we delineate a preliminary bounding box around each tree-top. Second, we refine the segmentation result by accurately delineating the crown boundaries. Let us focus on a generic k^{th} tree and on CHM_1. After a median filtering of the CHM, the J neighbouring tree-tops of $\mathbf{s}_k$ within a maximum radius r are detected, i.e., we select a subset of seeds $\{s_j\}_{j=1}^{J} \in \mathcal{S}$ such that:

$$\mathbf{s}_j \in \mathcal{S} \ : \ \|\mathbf{s}_k - \mathbf{s}_j\| \leq r \tag{8}$$

If no trees are found around $\mathbf{s}_k$ (i.e., the tree can be considered isolated), the method moves directly to the second phase. For each $\{\mathbf{s}_j\}_{j=1}^{J} \in \mathcal{S}$, we define line $\ell_{k,j}$ connecting $\mathbf{s}_k$ and $\mathbf{s}_j$ and the corresponding values of the CHM $\Upsilon_{k,j}$. We search for the absolute minimum of $\Upsilon_{k,j}$ and the corresponding x, y position in $\ell_{k,j}$. The 2-D line perpendicular to $\ell_{k,j}$ passing trough the x, y point corresponding to the minimum of $\Upsilon_{k,j}$ can be considered as a conservative crown boundary. By repeating this operation for all $\{\mathbf{s}_j\}_{j=1}^{J}$ we generate the preliminary bounding box of the k_{th} tree. The bounding box allows us to use the contextual information of the tree and its neighbours in the segmentation. Figure 3 illustrates the preliminary segmentation of a tree surrounded by three neighbours.

In the second phase of the segmentation we delineate the crown by analyzing the values of the CHM around the seed position $\mathbf{s}_k$. To this end, we apply a crown delineation algorithm similar to those proposed in [18], [19]. In greater detail, we analyze the profile of the canopy in several directions starting from the position of the tree-top. For each direction, we search for the first local minimum and its position is considered as a crown boundary reference point. It is worth noting that, to increase the reliability of the segmentation result, we consider only the crown boundary reference points that are inside the conservative bounding box delineated in the previous phase of the segmentation. Indeed, in some cases the first local minimum may be found further away than the true crown boundary point (e.g., due to the interpolation artifacts in the regularization step). The use of the bounding box allows us to reduce the probability of such errors by discarding large portions of the CHM that do not belong to the considered canopy. Finally, to define the final polygon of the segmented region, we compute the 2-D convex hull of the obtained set of reference crown boundary points. This is done because it is reasonable to approximate the crown perimeter as a 2-D convex polygon and in this way we discard the points that are inside the canopy perimeter but are wrongly detected as crown boundary. The outcomes of the segmentation are two sets of regions $\{R_{1,k}\}_{k=1}^{N}$ and $\{R_{2,k}\}_{k=1}^{N}$, where $R_{1,k}$ and $R_{2,k}$ delineate the crown of the tree $\mathbf{s}_k$ in CHM_1 and CHM_2, respectively. It is worth noting that all the areas that are not included in $\{R_{1,k}\}_{k=1}^{N}$ and $\{R_{2,k}\}_{k=1}^{N}$, and are not affected by large changes Ω_l, belong to the class ω_n.

In order to exploit the full information content of the LiDAR data we perform the detection of the single-tree changes directly in the point cloud domain. To this end, we transfer the sets of regions $\{R_{1,k}\}_{k=1}^{N}$ and $\{R_{2,k}\}_{k=1}^{N}$ to the 3-D point cloud space, generating two sets of segmented point clouds $\{C_{1,k}\}_{k=1}^{N}$ and $\{C_{2,k}\}_{k=1}^{N}$ where $C_{1,k}$ and $C_{2,k}$ represent the crown of the tree $\mathbf{s}_k$ at times t_1 and t_2, respectively. Since it is not feasible to compare the two point clouds $C_{1,k}$ and $C_{2,k}$ using a point-to-point approach, we reconstruct the external surface of the tree canopy at the two dates using an object-based approach defined by a parametric modeling. The 3-D model can be used to compute an estimate of the crown volume which is less affected by outliers with respects to other methods such as convex hull or alpha shape. It is worth noting that any model can be used in principle with the proposed technique but here we focus on conifer trees and thus a 3-D ellipsoid is suitable to accurately model the tree canopy [37]–[39]. The mathematical model of the generic k_{th} tree is defined by four parameters that control the shape of the ellipsoid: i) the tree-top height $H_{t,k}$, ii) the crown height $ch_{t,k}$, iii) the crown radius $cr_{t,k}$, iv) the crown curvature $cc_{t,k}$, with $t = 1, 2$. The 3-D model is defined as follows:

$$\frac{(z + ch_{t,k} - H_{t,k})^{cc_{t,k}}}{{ch_{t,k}}^{cc_{t,k}}} + \frac{\left[(x - x_k)^2 + (y - y_k)^2\right]^{cc_{t,k}/2}}{{cr_{t,k}}^{cc_{t,k}}} = 1$$
$$H_{t,k} - ch_{t,k} < z < H_{t,k}, \ t = 1, 2 \tag{9}$$

Figure 4 shows an example of the 3-D ellipsoids with the described parameters. To define the two 3-D ellipsoids for

both point clouds $C_{1,k}$ and $C_{2,k}$, we need to estimate the aforementioned parameters at both dates. Due to the conservative crown segmentation, the number of outliers in the segmented point clouds $C_{1,k}$ and $C_{2,k}$ is reduced, thus making the parameter estimation process more reliable. Since we are in a multitemporal framework, we perform the estimation by fusing the information of both dates to improve the accuracy of the estimates at single date. To this end, we define a set of rules based on natural physical constraints. First, we estimate the tree-top heights $H_{1,k}$ and $H_{2,k}$ as the highest elevation values of the two point clouds $C_{1,k}$ and $C_{2,k}$, respectively. It is very unlikely that tree-top height decreases over time except some cases in which the highest part of the tree is damaged (e.g., due to severe whether conditions). Thus, we assume that $H_{1,k} \leq H_{2,k}$ and if this condition is not satisfied we set $H_{1,k} = H_{2,k}$.

Then, we estimate the crown base heights $bh_{1,k}$ and $bh_{2,k}$ (i.e., heights of the lowest branch) defined as $bh_{t,k} = H_{t,k} - ch_{t,k}$, $(t = 1, 2)$. The estimates are obtained by analyzing the vertical profiles of the segmented point clouds. If the two point clouds have been acquired few years apart, we can assume that the base height does not variate significantly with time (i.e., $bh_{1,k} = bh_{2,k} = bh_k$). Indeed, the base height variation (i.e., rise of the lowest branch of the tree) is due to the death of the lowest branches of the canopy [40] and thus it does not change rapidly. Accordingly, we can define a single base height as $bh_k = \min\{bh_{1,k}, bh_{2,k}\}$. In this way we improve the estimation of the base height by fusing the information of the multitemporal LiDAR data. Indeed, the laser may penetrate more the lower portion of the canopy at one of the two dates with respect to the other due to a higher pulse density thus allowing for a more accurate estimation. By fusing the two estimates we use the higher density data to improve the estimation in the other one. It is worth noting that if the time difference between the acquisitions of the two LiDAR data is large, this assumption is not valid anymore and the base heights have to be estimated separately at the two dates. The two crown heights can be computed as $ch_{t,k} = H_{t,k} - bh_k$, $t = 1, 2$.

To estimate the crown radius, for each segmented tree we select all the points belonging to the canopy (i.e., points for which $z > bh_k$) and then we compute the area $A_{t,k}$ of the 2-D convex hull computed using the x, y coordinates of the selected points. Finally, we calculate the crown radius as $cr_{t,k} = \sqrt{A_{t,k}/\pi}$, $t = 1, 2$. Also in this case we use the multitemporal information to improve the estimation accuracy. To this end, we consider the constraint on the radius $cr_{1,k} \leq cr_{2,k}$. In particular, for those crowns where $cr_{1,k} > cr_{2,k}$ we set $cr_{1,k} = cr_{2,k}$ since it is plausible to assume that the crown radius does not decrease in time.

Similarly to the base height, it is reasonable to assume that the crown curvature does not change significantly in time (i.e., $cc_{1,k} = cc_{2,k} = cc_k$). Thus, the crown curvature cc_k is estimated by detecting the one that minimizes a residual distance metric between the 3-D ellipsoid and the points belonging to the external surface of the segmented point cloud with the highest number of points. If we consider the crown at time t_1 as the crown with larger number P of points, we can define the residual distance metric of a single x_i, y_i, z_i point for a given cc'_k as:

$$r_i(cc'_k) = \frac{(z_i + ch_{1,k} - H_{1,k})^{cc'_k}}{{ch_{1,k}}^{cc'_k}} + \frac{\left[(x_i - x_k)^2 + (y_i - y_k)^2\right]^{cc'_k/2}}{{cr_{1,k}}^{cc'_k}} - 1. \tag{10}$$

Thus, the overall residual distance metric for P points can be defined as:

$$r(cc'_k) = \sum_{i=1}^{P} r_i(cc'_k)^2 \tag{11}$$

The estimate of cc_k is selected according to:

$$cc_k = \underset{cc'_k}{\operatorname{argmin}}\, r(cc'_k). \tag{12}$$

The aforementioned operations allow us to simplify the detection of the 3-D changes at the individual tree level (in particular the detection of the crown volume growth dV) by characterizing the canopy structure using a 3-D ellipsoid regardless of the pulse density. For each k_{th} tree, we have the following variables:

- tree-top heights $H_{1,k}$ and $H_{2,k}$;
- two 3-D ellipsoids $E_{1,k}$ and $E_{2,k}$ (defined using $H_{t,k}$, $cr_{t,k}$, $ch_{t,k}$, cc_k, $t = 1, 2$) representing the canopy structure at the two dates.

The vertical growth of the considered tree can be computed as $dH_k = H_{2,k} - H_{1,k}$. In order to compute the crown volume growth, first we compute the volume of the considered tree at the two dates according to:

$$V(E_{t,k}) = \iint\limits_{\sqrt{x^2+y^2} \leq cr_{t,k}} \left(ch_{t,k}^{cc_k} + \frac{(x^2+y^2)^{cc_k/2}}{cr_{t,k}^{cc_k}} \cdot ch_{t,k}^{cc_k} \right)^{1/cc_k} - ch_{t,k} + H_{t,k}\, dx\, dy,\ t = 1,\ 2. \tag{13}$$

Then, the crown volume growth is estimated as:

$$dV_k = V(E_{2,k}) - V(E_{1,k}). \tag{14}$$

It is now possible to distinguish between trees with no growth (class ω_{ng}) and trees with growth (class ω_g) by applying two thresholds to dH_k and dV_k, i.e,:

$$\mathbf{s}_k \in \begin{cases} \omega_{ng} & dH_k < t_{dH} \wedge dV_k < t_{dV} \\ \omega_g & dH_k \geq t_{dH} \vee dV_k \geq t_{dV} \end{cases}. \tag{15}$$

We used these thresholds to avoid the effects of small differences that may depend on either systematic acquisition errors of LiDAR or the complex forest scenario. Thus, the thresholds allow us to correctly identify the trees that show a significant growth. From the definition of dH_k and dV_k, one can see that these two attributes are not mutually exclusive since both $H_{t,k}$, $(t = 1, 2)$ and $E_{t,k}$, $(t = 1, 2)$ are dependent from $ch_{t,k}$, $(t = 1, 2)$.

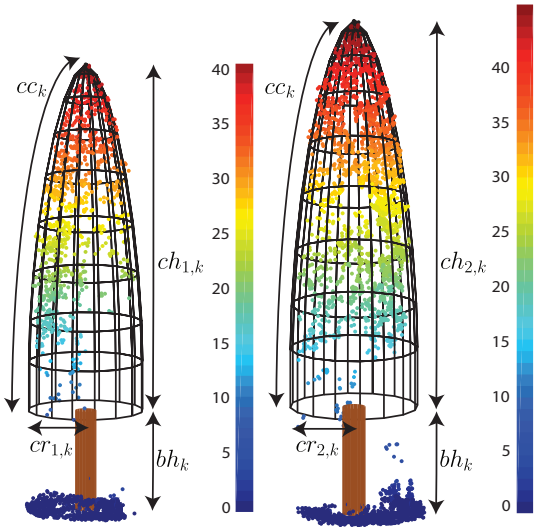

(a) $C_{1,k}$ and $E_{1,k}$ (b) $C_{2,k}$ and $E_{2,k}$

Fig. 4: 3-D models fitted on the segmented point clouds at the two dates for a generic tree k.

III. Experimental Results

A. Dataset Description and Experimental Setup

To assess the effectiveness of the proposed method, we performed the CD analysis on two forest areas located in the southern Italian Alps in the Trento province. The first area is located in Baselga di Piné, Trentino (central point coordinates $46°10'79,18''N, 11°22'66,13''E$) and extends approximately $25\,ha$. The terrain is characterized by a complex morphology with an altitude ranging from $850\,m$ to $1000\,m$. The species composition of the forest is mainly Larix decidua (European Larch) and Picea abies (Norway Spruce). The LiDAR data were acquired in 2010 and 2014 by an ALTM 3100EA sensor with a maximum pulse density of $10\,pls/m^2$ and $15\,pls/m^2$, respectively, and four returns registered for each pulse. We selected two $70\,m \times 70\,m$ areas (see Figures 5a-5e and 5b-5f) for our experiments.

The second study area is an old-growth coniferous forest located in Pellizzano, Trentino (central point coordinates $46°17'31,00''$N, $10°45'56,49''$E). The size of the area is $3200\,ha$ with an altitude ranging from $900\,m$ to $2800\,m$ and a complex terrain morphology. The species composition is similar to the one of the first test forest. The LiDAR data were acquired in 2012 by a Riegl LMS-Q680i sensor with a maximum pulse density of $50\,pls/m^2$ and in 2015 by an ALTM 3100EA sensor with a maximum pulse density of $15\,pls/m^2$. In both the acquisitions four returns were registered for each pulse. We selected a $70\,m \times 70\,m$ area (Figures 5c-5g) and a $80\,m \times 80\,m$ area (Figure 5d-5h) for our experiments.

Table I shows the parameters of the proposed method used for all the considered LiDAR point clouds. To generate the CHMs, we considered a spatial resolution of $0.3\,m$ to accurately represents the forest structure. Accordingly, the radius of the structuring element (with the shape of a disk) was set to 3 and the large changes area threshold t_A was set equal to 100 pixels (i.e., minimum large changes area $9\,m^2$) in order to avoid the detection of the crown widths variations as large changes. For the detection of the tree-tops a small 3×3 median kernel filter and a 4×4 Gaussian kernel filter were considered to reduce the missed detection of trees present in the scene, even though this increases the false alarm rate. However, due to the synergistic use of the of multitemporal data, the false alarm rate is reduced by comparing the sets of seeds. The distance threshold t_s for the matching was set to $1.5\,m$ in order to be robust to the presence of residual registration errors or variations of the tree-top position due to natural causes.

For the segmentation we selected a larger 5×5 kernel filter to avoid the detection of local minima caused by errors in the regularization step. The preliminary segmentation is carried out analyzing a maximum of $J = 4$ neighbours trees (selected according to the typical structure of the forest) in a range of $r = 10\,m$ from the considered tree. The minimum canopy height growth t_{dH} and minimum crown volume growth t_{dV} were set to $0.2\,m$ and $10\,m^3$ considering the time interval between the two acquisitions. Note that we used the same parameters for all the considered LiDAR data even if they are characterized by very different pulse densities and represent forests with very diverse characteristics. This choice of parameters can be considered general for Alpine forest. It is worth noting that a minimum pulse density of $5\,pls/m^2$ is required in order carry out an accurate CD.

The first step of the method is the ICP registration. Since the data were already registered, to validate the ICP algorithm with the used settings we simulated different registration errors and analyzed the registration results using Ground Control Points (GCPs). In greater detail, for each stand we tested shift errors ranging from $0\,m$ to $10\,m$. For each shift we selected two partially overlapping portions of the data (one at time t_1 and one at time t_2) with the same size and we shifted data at time t_2 in such a way that they completely overlap. To test also the robustness to rotation errors we added different amounts of rotation (from $0°$ to $5°$). We validated the results both from a qualitative (by visual analysis of the registered point cloud and the reference data) and quantitative (using GCPs) point of view. We selected as GCPs the position of the tree-tops at the two dates and we manually matched the tree-top at time t_1 with the tree-tops at time t_2. For each test we applied the corresponding shift and rotation to the GCPs and after the ICP step (applied to the shifted point cloud) we applied the resulting rigid transformation on the GCPs of time t_2. Finally, we computed the average Euclidean distance between the tree-tops at time t_1 and the registered tree-tops at time t_2. The results of the detection of large changes have been validated by using reference maps derived by photo-interpretation. The reference maps were then compared with the ones automatically generated by the proposed method. The validation of the tree detection has been carried out by using a map of trees identified by a visual analysis. In particular, the obtained results were evaluated in terms of false alarms and missed alarms. We manually estimated the crown radius and crown base height for 72 trees in stand S1, 80 trees in stand S2, 16 trees in stand S3 and 36 trees in stand S4. The segmentation results have been validated both qualitatively by visual analysis

TABLE I: Parameter values defined for the proposed method.

Parameter	Value
Percentile P_r	70^{th}
Resolution of CHM and DSM	$0.3\,m$
Height Threshold (ω_{lp}) $t_{h,lp}$	$3\,m$
Height Threshold (ω_{ln}) $t_{h,ln}$	$5\,m$
Structuring Element Radius	3
Area Threshold t_A	100
Median Kernel Size (tree detection)	3×3
Gaussian Kernel Size (tree detection)	4×4
Gaussian Filter Standard Deviation	4
Matching Threshold t_s	$1.5\,m$
Median Kernel Size (crown delineation)	5×5
Number of Neighbours Trees J	4
Search Radius for Neighbours Trees r	$10\,m$
Minimum Height Growth t_{dH}	$0.2\,m$
Minimum Crown Volume Growth t_{dV}	$10\,m^3$

of the segmented point clouds and quantitatively by comparing the true radii with the estimated ones. We computed the Mean Absolute Error (MAE), the Root Mean Square Error (RMSE), the Normalized Mean Square Error (NRMSE) and the coefficient of determination (R^2) for both the radius and base height estimations. Finally, the single-tree changes results were evaluated by a team of experts of the regional forest service.

B. Results and Discussion

Figures 6 and 7 show the results obtained in the ICP step in terms of residual mean Euclidean distance on the GCPs at times t_1 and t_2. In the case of no artificial rotation, Figure 6a shows that the the proposed ICP procedure can accurately register data up to a shift of $4\,m$ for all the stands and up to $7\,m$ for the stand $S4$. On the contrary, the standard ICP procedure (Figure 6b) is robust to shift up to $3\,m$. At a shift of $4\,m$ the residual error becomes significant for the stand S3. Figure 7 shows the results with different amounts of shift and an applied rotation ranging from 0° to 5° degrees. Figures 7a, 7c, 7e, 7g shows that the proposed ICP procedure is robust also to rotation errors since it reaches almost equal results with different combination of shift and rotation. Figures 7b, 7d, 7f, 7h point out that the standard ICP procedure shows stable results at different rotation but is more sensible to shift errors.

Let us focus the attention on the detection of large changes $\Omega_l = \{\omega_{ln}, \omega_{lp}\}$. Figure 8 shows a qualitative example of how morphological operators remove the noise from the CD map. The erosion filter and the threshold on the area of the large changes allow us both to discard the false alarms due to noise in the CHMs and to remove the pixels representing the expansion of the tree crowns. These qualitative results are confirmed by the quantitative evaluation given in Table II. In the considered forest areas, only deforestation changes (i.e., large negative changes ω_{ln}) are present. The three confusion matrices show good detection accuracy with a small number of missed and false alarms. Note that no large changes were present in stand S2 and the proposed technique did not detect any false alarm.

TABLE II: Confusion matrices related to the detection of large negative changes ω_{ln} in terms of classified pixels in the CHM for stands S1, S3 and S4.

(a) S1

		Estimated	
		Change	No change
True	Change	531	34
	No change	19	54172

(b) S3

		Estimated	
		Change	No change
True	Change	959	56
	No change	98	53877

(c) S4

		Estimated	
		Change	No change
True	Change	1453	103
	No change	186	69547

After having identified the large changes, we focus the attention on the changes at the individual tree level. Figure 9 shows a qualitative example of the tree-top detection. Note how the synergistic use of the multitemporal information allows us to discard false alarms (i.e., the red dot identified only at time t_2.). Table III presents the detection accuracy, the number of missed trees and false trees. By matching the two set of seeds, we reduced the false alarm rate from $5.5\% - 4.9\%$ to 1.7% without affecting the detection accuracy and the missed alarm rate. This shows that the method in most of the cases correctly distinguishes between trees that have been detected only at one date and false alarms. The false alarms that are not discarded during the matching are mostly due to steeply inclined tree branches that generate a peak in the CHM. The analysis of the missed alarm rate shows that there is almost no improvement after the matching. This is due to two main reasons : i) the tree has not been identified at both dates and thus it is not possible to exploit the multitemporal information to recover it; ii) the tree-top is covered by dominant trees.

At the end of the tree detection part, we move to the crown delineation. Figure 10 shows the scatter plots and error metrics for the estimated crown radius at the two dates. The plots show the effectiveness of the proposed segmentation method which accurately segments the tree crowns and estimates the crown radius. Thus, the coefficient of determination R^2 shows quite high values at both dates ($R^2 = 0.72$ at time t_1 and $R^2 = 0.72$ at time t_2). In addition, the visual analysis (see Figure 11) of the segmented point clouds confirms the accuracy of the segmentation results. To validate the 3-D model used to represent the structure of the crown, we evaluate the bh estimation (Figure 12). In particular, Figures 12a and 12b show the results obtained when the estimation is carried out at the single date, while Figure 12c shows the base height estimated by fusing the multitemporal data. As one can see in Figure 12, the base height estimation at time t_2 is less accurate than the one obtained at time t_1 since the LiDAR data acquired

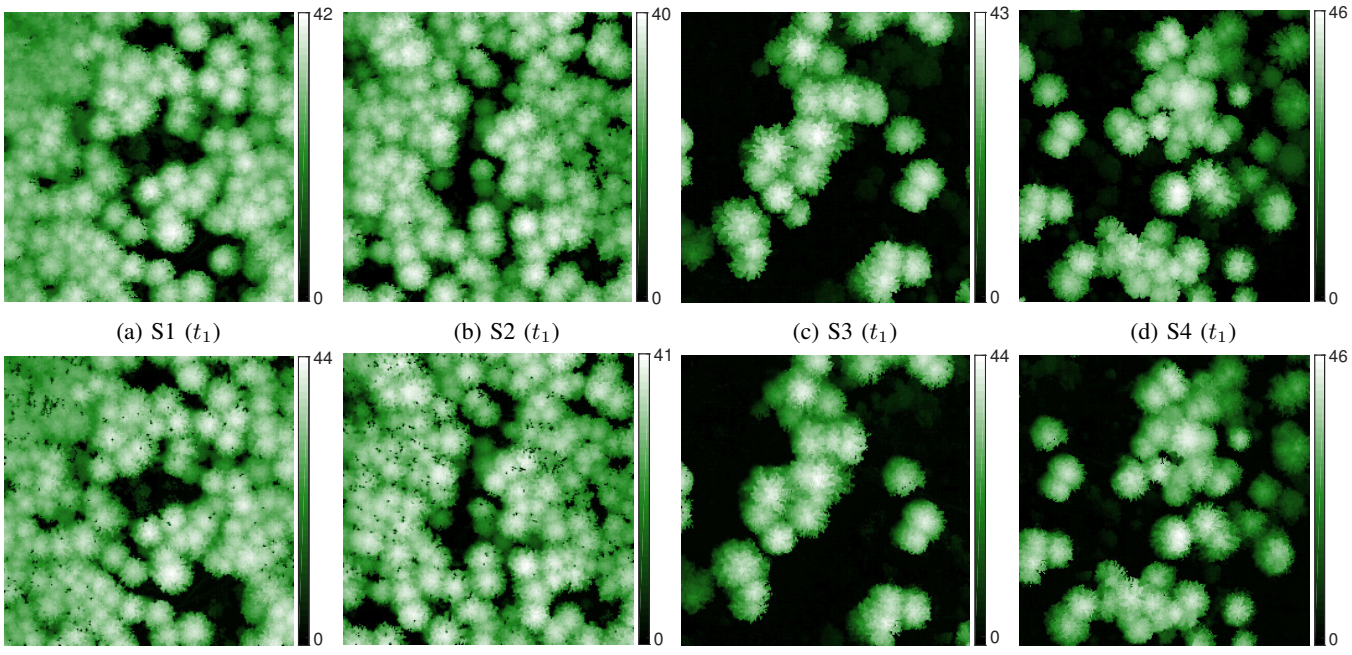

(a) S1 (t_1) (b) S2 (t_1) (c) S3 (t_1) (d) S4 (t_1)

(e) S1 (t_2) (f) S2 (t_2) (g) S3 (t_2) (h) S4 (t_2)

Fig. 5: CHMs of the 4 stand plots at times t_1 and t_2. The considered forest stands are characterized by different forest densities and terrain morphologies. The rasterization has been carried out at $0.3\,m$ resolution.

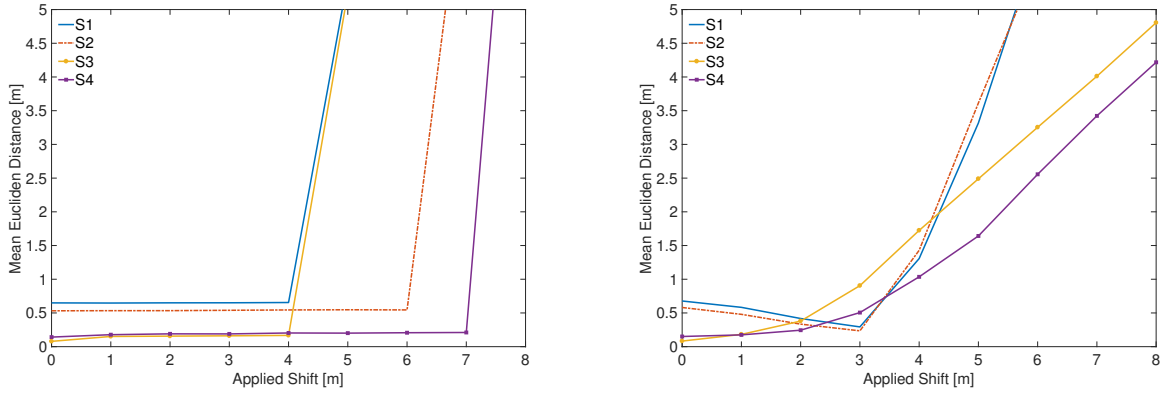

(a) (b)

Fig. 6: Plots showing the residual registration error (on the GCPs) versus the amount of artificially introduced shift. The x-axis represents the applied shift while the y-axis corresponds to the residual error: (a) proposed ICP procedure; (b) standard ICP procedure.

at time t_2 (on both the study areas) are characterized by a smaller pulse density that result in a lower penetration rate of the laser in the lower portion of the canopy, thus making the base height estimation less reliable. However, Figure 12c shows that by fusing the multitemporal information of the two acquisitions we can improve the base height estimation with respect to each single date. Indeed, we improved the coefficient of determination from $R^2 = 0.79$ (at time t_1) and $R^2 = 0.66$ (at time t_2) to $R^2 = 0.81$. It is worth noting that, even though the denser point cloud can be used to improve the crown parameter estimation on the other point cloud, a lower bound on the point density for the applicability of the method should be identified. If the point density of both the point clouds is too low the crown parameters will be inaccurately estimated at both dates. A reasonable lower bound on the pulse density is $5\,pls/m^2$.

TABLE III: Detection accuracy, false alarms and missed alarms obtained by the proposed method for the tree-top detection in all the four considered stands.

	Detection accuracy	False alarms	Missed alarms
t_1	337 (98%)	19 (5.5%)	7 (2%)
t_2	335 (97.4%)	17 (4.9%)	9 (2.6%)
Matching	336 (97.7%)	6 (1.7%)	8 (2.3%)

The final step of the proposed hierarchical CD method performs multitemporal analysis at the individual tree level to detect and quantify the single-tree changes. Figure 13 shows,

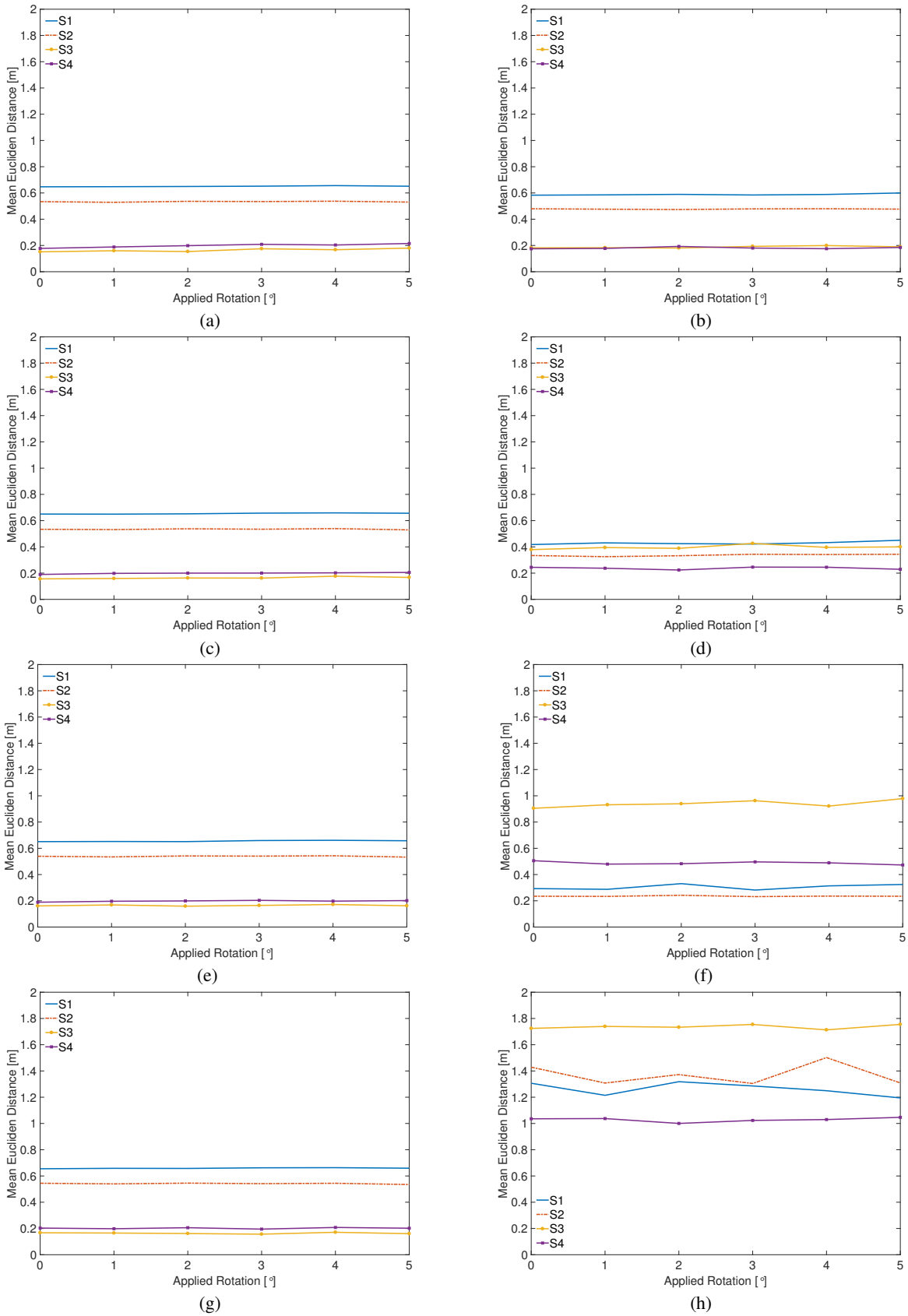

Fig. 7: Plots showing the residual registration error (on the GCPs) versus the amount of artificially introduced rotation for different shifts: (a-c-d-e) proposed ICP procedure with an applied shift of $1, 2, 3, 4\,m$, respectively; (b-d-f-h) standard ICP procedure with an applied shift of $1, 2, 3, 4\,m$ respectively.

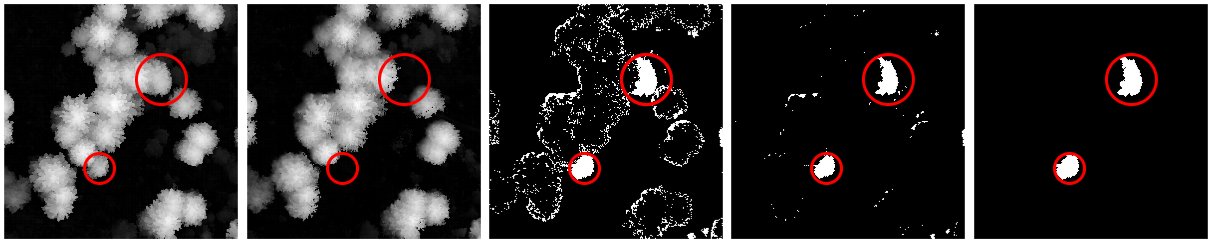

(a) (b) (c) (d) (e)

Fig. 8: Example of the detection of large changes for stand S3 (the red circles highlight the large changes identified by photo-interpretation): (a)-(b)CHMs at times t_1 and t_2; (c) binary difference image of the two CHMs after the thresholding operation; (d) binary map after the erosion morphological filter; (e) final result after the elimination of small patches and the dilation filter.

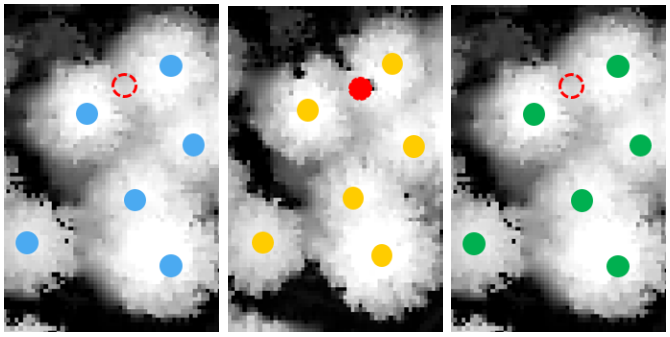

(a) $\mathcal{S}_1 = \{s_{1,k_1}\}_{k_1=1}^{N_1}$ (b) $\mathcal{S}_2 = \{s_{2,k_2}\}_{k_2=1}^{N_2}$ (c) $\mathcal{S} = \{s_k\}_{k=1}^{N}$

Fig. 9: Example of tree-top detection on a small portion of the CHM: (a) set of seeds $\mathcal{S}_1$ identified at time t_1; (b) set of seeds $\mathcal{S}_2$ identified at time t_2; (c) set of matched seeds $\mathcal{S}$. The detection at time t_2 identified a false alarm (red dot) which has not been identified at time t_1 (red dashed line) and thus it is correctly discarded by the matching.

TABLE IV: Statistics of the individual tree parameters for each stands at both dates and in terms of: (a) dH; (b) dV.

(a)

Stand	Top height $[m]$ t_1		Top height $[m]$ t_2		dH $[m]$	
	Range	Mean	Range	Mean	Range	Mean
S1	16.9-42.9	35.2	18.3-44.1	36.2	0-2.8	1
S2	18.7-40.6	33.4	19.5-41.5	34.3	0-2.7	0.9
S3	6.8-41.7	33.9	7.2-41.8	34.4	0-2.5	0.4
S4	21-46.2	36.5	21.3-46.4	36.7	0-0.7	0.3

(b)

Stand	Crown Volume $[m^3]$ t_1		Crown Volume $[m^3]$ t_2		dV $[m^3]$	
	Range	Mean	Range	Mean	Range	Mean
S1	53-1200	431	54-1237	463	0-93	31
S2	55-1265	345	73-1284	373	0-95	27
S3	57-2394	1044	88-2410	1058	0-42	14
S4	150-2160	987	150-2179	1004	0-67	15

for each stand, the map with the corresponding identified classes, whereas Figure 14 shows a qualitative example of the object-based change detection of a single-tree. Table IV shows the statistics of the top height and crown volume for each stand together with the corresponding dH and dV statistics. It is worth noting that the statistics of the single-tree changes have been computed considering both the trees in ω_{ng} and ω_g. Focusing on the vertical growth showed in Table IVa, we can observe a different behavior in stands S1 and S2 and stands S3 and S4. Indeed, stands S3 and S4 show a vertical growth with a mean variation of $0.4\,m$ and $0.3\,m$, respectively, whereas stands S1 and S2 show a vertical growth of $1\,m$ and $0.9\,m$, respectively. These results are in agreement with the expectation of the team of experts of the forest service since stands S3 and S4 are characterized by older trees with respect to stands S1 and S2. Indeed, it is well know that the age of the tree influences its growth rate which decreases as the age of the tree increases. This observation can be extended also to the crown volume variation. Table IVb shows that in stands S1 and S2 there is a larger variation in terms of crown volume growth with respect to stands S3 and S4 (i.e., mean variation of $31\,m^3$ and $27\,m^3$, respectively). Moreover, Figure 13 shows that for stands S3 and S4 there is a larger number of trees that do not show significant growth (i.e., belong to class ω_{ng}) with respect to stands S1 and S2. Note that stands S1 and S2 have very similar characteristics in terms of forest structure (see Figures 5a and 5b); this is also true for stands S3 and S4 (Figures 5c and 5d). This condition affects the single-tree changes since stands with similar characteristics show similar value of vertical and crown volume growth.

IV. Conclusion

In this work we have presented a method for the detection of 3-D changes in forest areas using multitemporal LiDAR data. The method first detects the large changes and then focuses on the individual tree canopy in order to detect the single-tree changes by means of an object-based CD. The object-based CD identifies both the vertical and the crown volume growth of each single-tree.

The experimental results confirmed the effectiveness of the proposed method. The large changes were accurately identified in all the considered stands with low false and missed alarm

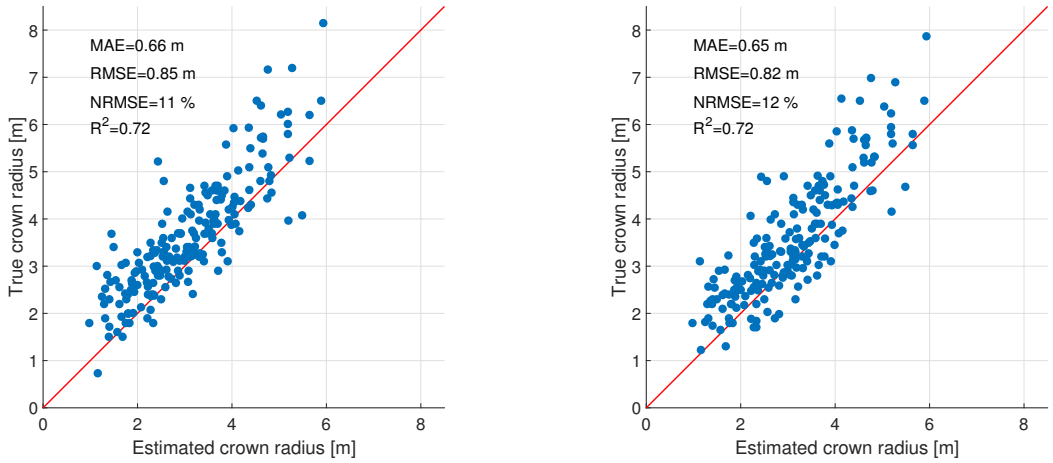

(a) (b)

Fig. 10: True versus estimated crown radius (cr) for all the considered stands at the two dates: (a) time t_1, (b) time t_2.

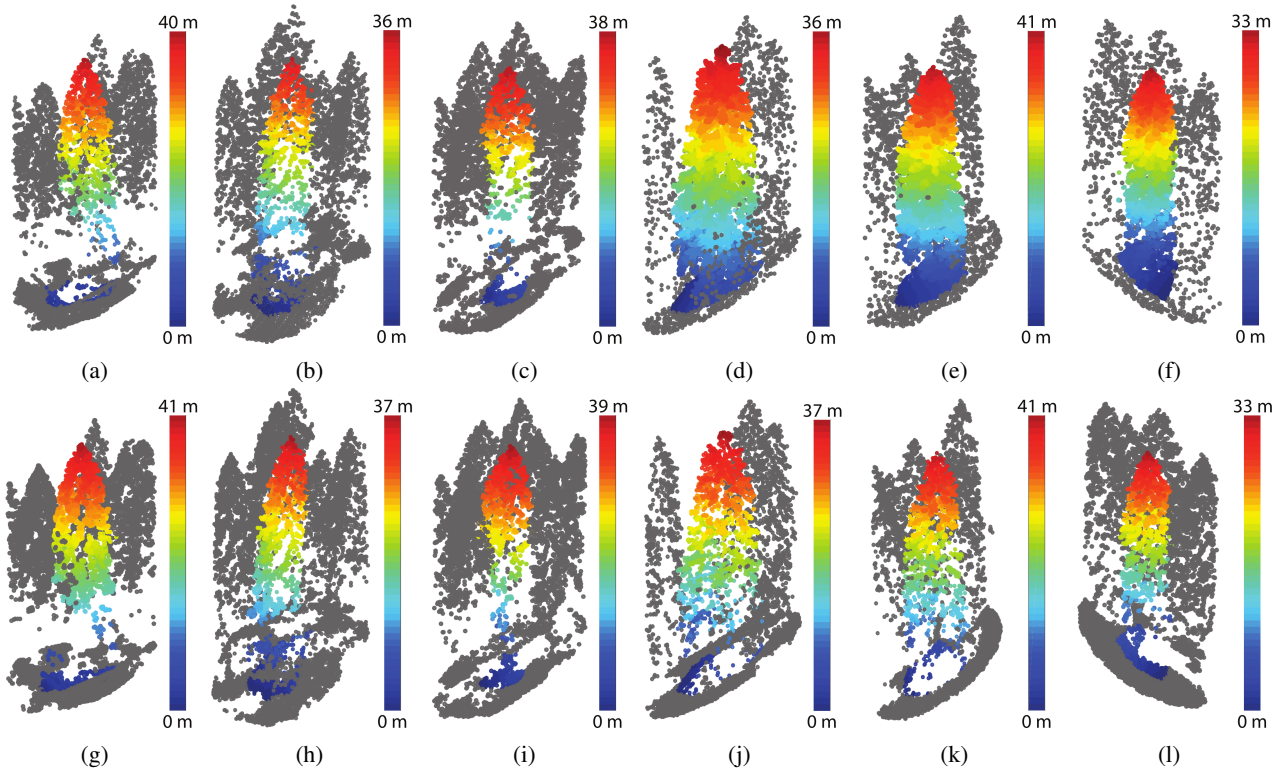

(a) (b) (c) (d) (e) (f)

(g) (h) (i) (j) (k) (l)

Fig. 11: Qualitative examples of delineated tree canopies obtained by the proposed crown following approach (the segmented crowns are displayed in bright colors): (a-f) segmented crowns at time t_1; (g-l) segmented crowns at time t_2.

rates. In the tree detection phase, after the matching we jointly use the multitemporal LiDAR data in order to discard the false alarms and recover some of the tree-tops identified only at one date, thus reducing the number of false alarms (from $4.9-5.5\%$ to 1.7%) without significantly increasing the number of missed alarms (from $2-2.6\%$ to 2.3%). Regarding the canopy characterization, we used a 3-D ellipsoid model in order to reconstruct the canopy structure considering the multitemporal information to improve the parameters estimation accuracy. The comparison between estimated parameters and the true parameters pointed out that the method estimated the crown radius with an R^2 of 0.72 at both dates. The base height estimation performed at the single date showed good performance at time t_1 with an R^2 of 0.79, whereas at time t_2 the estimation was significantly less accurate with an R^2 of 0.66. However, by fusing the information of the two dates we reduced the effect of the low penetration of the laser in the lower portion of some canopies thus improving the estimation reaching an R^2 of 0.81. By means of the 3D ellipsoid, we computed the vertical growth ω_{dH} and crown volume growth ω_{dV} for each tree. The statistics of these changes were consistent with what expected by the experts

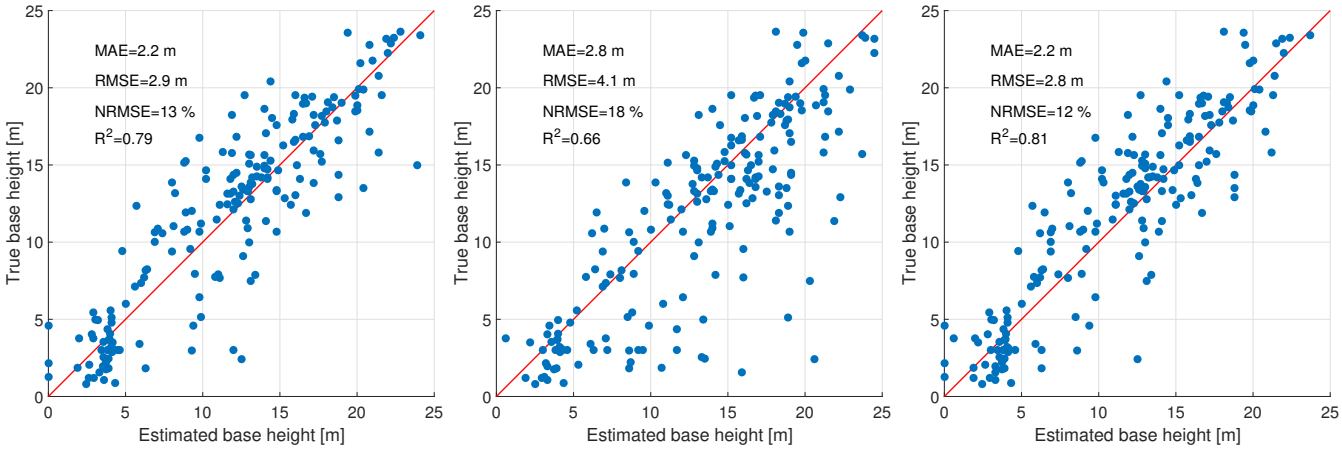

(a) (b) (c)

Fig. 12: True versus estimated base height (bh) for all the considered stands: (a) single date estimation at time t_1, (b) single date estimation at time t_2, (c) multitemporal estimation.

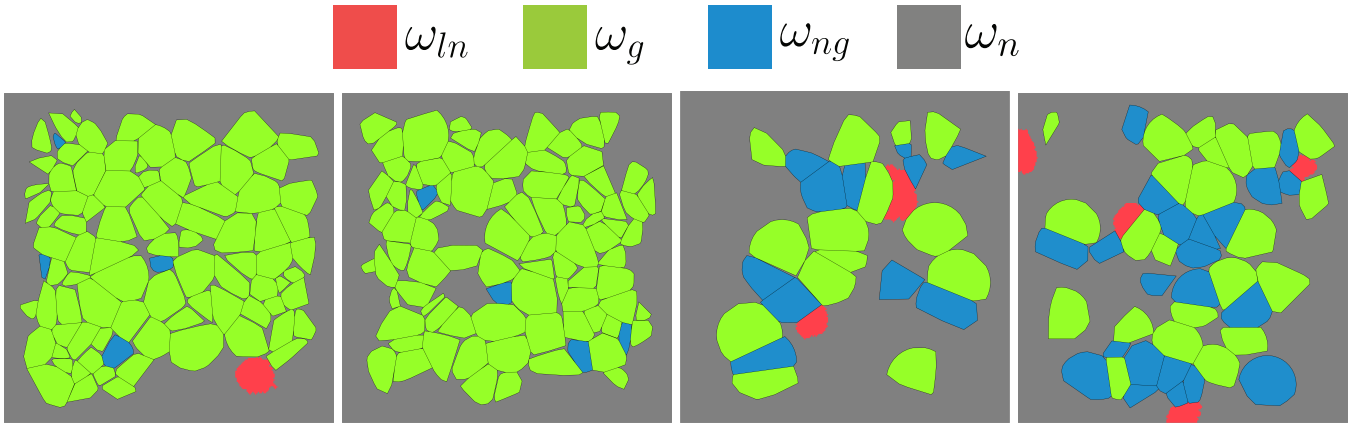

(a) S1 (b) S2 (c) S3 (d) S4

Fig. 13: Maps representing the different kinds of changes identified in the considered stands. (i.e., ω_{ln} large negative changes, ω_g trees with significant growth, ω_{ng} trees with no significant growth, ω_n areas of no interest for forest studies,)

of the regional forest service according to the properties of the analyzed stands. In particular, stands S1 and S2 showed a larger vertical growth (i.e., $1 - 0.9\,m$) with respect to stands S3 and S4 ($0.4 - 0.3\,m$) which are characterized by older trees. The crown volume growth showed similar results with the first two stands characterized by a growth of $31\,m^3$ and $27\,m^3$, respectively. One of the most important properties of the proposed method is that it can effectively compare LiDAR data with different pulse densities. However, for an accurate characterization of the tree growth the lower bound on each single date density is of $5\,pls/m^2$.

As future developments of this work, we plan to extend the detection of single-tree changes to analyze the variation of biomass in order to better characterize the health status of the forest and to test the proposed method on forests with younger trees to analyze the growth rate of trees with very different ages. Finally, we plan to use convex hull and alpha shape in order to characterize more the canopy structure and thus its changes.

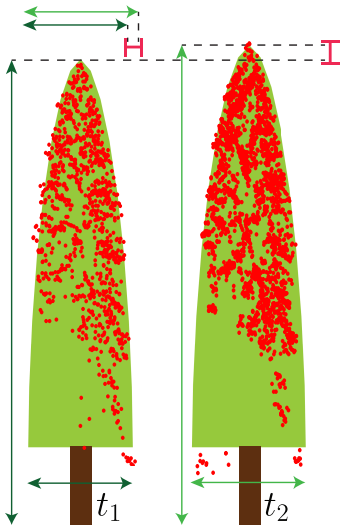

Fig. 14: Real example of CD at the individual tree level showing the 3-D model (with the two related segmented point clouds in red). Note the height and horizontal growth that contribute to the crown volume variation.

APPENDIX A
NOTATION

The notation used in this paper is shown in Table V.

REFERENCES

[1] J. G. Lyon, D. Yuan, R. S. Lunetta, and C. D. Elvidge, "A change detection experiment using vegetation indices," *Photogrammetric Engineering and Remote Sensing*, vol. 64, no. 2, pp. 143–150, 1998.

[2] V. Walter, "Object-based classification of remote sensing data for change detection," *{ISPRS} Journal of Photogrammetry and Remote Sensing*, vol. 58, no. 3, pp. 225–238, 2004.

[3] B. Desclée, P. Bogaert, and P. Defourny, "Forest change detection by statistical object-based method," *Remote Sensing of Environment*, vol. 102, no. 1, pp. 1–11, 2006.

[4] P. Coppin, I. Jonckheere, K. Nackaerts, B. Muys, and E. Lambin, "Review article digital change detection methods in ecosystem monitoring: a review," *International journal of remote sensing*, vol. 25, no. 9, pp. 1565–1596, 2004.

[5] F. Bovolo and L. Bruzzone, "A theoretical framework for unsupervised change detection based on change vector analysis in the polar domain," *IEEE Transactions on Geoscience and Remote Sensing*, vol. 45, no. 1, pp. 218–236, Jan 2007.

[6] V. Meyer, S. S. Saatchi, J. Chave, J. W. Dalling, S. Bohlman, G. A. Fricker, C. Robinson, M. Neumann, and S. Hubbell, "Detecting tropical forest biomass dynamics from repeated airborne lidar measurements," *Biogeosciences*, vol. 10, no. 8, pp. 5421–5438, 2013.

[7] H.-E. Andersen, S. E. Reutebuch, R. J. McGaughey, M. V. d'Oliveira, and M. Keller, "Monitoring selective logging in western amazonia with repeat lidar flights," *Remote Sensing of Environment*, vol. 151, pp. 157–165, 2014.

[8] M. Réjou-Méchain, B. Tymen, L. Blanc, S. Fauset, T. R. Feldpausch, A. Monteagudo, O. L. Phillips, H. Richard, and J. Chave, "Using repeated small-footprint lidar acquisitions to infer spatial and temporal variations of a high-biomass neotropical forest," *Remote Sensing of Environment*, vol. 169, pp. 93–101, 2015.

[9] S. Solberg, E. Næsset, K. H. Hanssen, and E. Christiansen, "Mapping defoliation during a severe insect attack on scots pine using airborne laser scanning," *Remote Sensing of Environment*, vol. 102, no. 3–4, pp. 364 – 376, 2006.

[10] B. St-Onge and U. Vepakomma, "Assessing forest gap dynamics and growth using multi-temporal laser-scanner data," *Power*, vol. 140, p. 200uJ, 2004.

[11] X. Yu, J. Hyyppä, H. Kaartinen, and M. Maltamo, "Automatic detection of harvested trees and determination of forest growth using airborne laser scanning," *Remote Sensing of Environment*, vol. 90, no. 4, pp. 451–462, 2004.

[12] M. Vastaranta, I. Korpela, A. Uotila, A. Hovi, and M. Holopainen, "Mapping of snow-damaged trees based on bitemporal airborne lidar data," *European Journal of Forest Research*, vol. 131, no. 4, pp. 1217–1228, 2012.

[13] U. Vepakomma, D. Kneeshaw, and B. St-Onge, "Interactions of multiple disturbances in shaping boreal forest dynamics: a spatially explicit analysis using multi-temporal lidar data and high-resolution imagery," *Journal of Ecology*, vol. 98, no. 3, pp. 526–539, 2010.

[14] U. Vepakomma, B. St-Onge, and D. Kneeshaw, "Spatially explicit characterization of boreal forest gap dynamics using multi-temporal lidar data," *Remote Sensing of Environment*, vol. 112, no. 5, pp. 2326–2340, 2008.

[15] A. Persson, J. Holmgren, and U. Söderman, "Detecting and measuring individual trees using an airborne laser scanner," *Photogrammetric Engineering and Remote Sensing*, vol. 68, no. 9, pp. 925–932, 2002.

[16] L. Duncanson, B. Cook, G. Hurtt, and R. Dubayah, "An efficient, multi-layered crown delineation algorithm for mapping individual tree structure across multiple ecosystems," *Remote Sensing of Environment*, vol. 154, pp. 378 – 386, 2014.

[17] A. Ferraz, F. Bretar, S. Jacquemoud, G. Gonçalves, L. Pereira, M. Tomé, and P. Soares, "3-d mapping of a multi-layered mediterranean forest using {ALS} data," *Remote Sensing of Environment*, vol. 121, pp. 210 – 223, 2012.

[18] C. Paris, D. Valduga, and L. Bruzzone, "A hierarchical approach to three-dimensional segmentation of lidar data at single-tree level in a multilayered forest," *IEEE Transactions on Geoscience and Remote Sensing*, vol. 54, no. 7, pp. 4190–4203, July 2016.

[19] B. Koch, U. Heyder, and H. Weinacker, "Detection of individual tree crowns in airborne lidar data," *Photogrammetric Engineering & Remote Sensing*, vol. 72, no. 4, pp. 357–363, 2006.

[20] X. Yu, J. Hyyppä, A. Kukko, M. Maltamo, and H. Kaartinen, "Change detection techniques for canopy height growth measurements using airborne laser scanner data," *Photogrammetric Engineering & Remote Sensing*, vol. 72, no. 12, pp. 1339–1348, 2006.

[21] X. Yu, J. Hyyppä, H. Kaartinen, H. Hyyppä, M. Maltamo, and P. Rönnholm, "Measuring the growth of individual trees using multi-temporal airborne laser scanning point clouds," in *Proceedings of ISPRS Workshop Laser Scanning*, vol. 2005. Citeseer, 2005, pp. 204–208.

[22] U. Vepakomma, B. St-Onge, and D. Kneeshaw, "Response of a boreal forest to canopy opening: assessing vertical and lateral tree growth with multi-temporal lidar data," *Ecological Applications*, vol. 21, no. 1, pp. 99–121, 2011.

[23] S. Srinivasan, S. C. Popescu, M. Eriksson, R. D. Sheridan, and N.-W. Ku, "Multi-temporal terrestrial laser scanning for modeling tree biomass change," *Forest Ecology and Management*, vol. 318, pp. 304 – 317, 2014.

[24] W. Xiao, S. Xu, S. O. Elberink, and G. Vosselman, "Individual tree crown modeling and change detection from airborne lidar data," *IEEE Journal of Selected Topics in Applied Earth Observations and Remote Sensing*, vol. 9, no. 8, pp. 3467–3477, Aug 2016.

[25] P. J. Besl and H. D. McKay, "A method for registration of 3-d shapes," *IEEE Transactions on Pattern Analysis and Machine Intelligence*, vol. 14, no. 2, pp. 239–256, Feb 1992.

[26] D. F. Huber and M. Hebert, "3d modeling using a statistical sensor model and stochastic search," in *2003 IEEE Computer Society Conference on Computer Vision and Pattern Recognition, 2003. Proceedings.*, vol. 1, June 2003, pp. I–858–I–865 vol.1.

[27] A. Myronenko and X. Song, "Point set registration: Coherent point drift," *IEEE Transactions on Pattern Analysis and Machine Intelligence*, vol. 32, no. 12, pp. 2262–2275, Dec 2010.

[28] B. Douillard, A. Quadros, P. Morton, J. P. Underwood, M. D. Deuge, S. Hugosson, M. Hallström, and T. Bailey, "Scan segments matching for pairwise 3d alignment," in *2012 IEEE International Conference on Robotics and Automation*, May 2012, pp. 3033–3040.

[29] G. C. Sharp, S. W. Lee, and D. K. Wehe, "Icp registration using invariant features," *IEEE Transactions on Pattern Analysis and Machine Intelligence*, vol. 24, no. 1, pp. 90–102, Jan 2002.

[30] J. Ho, A. Peter, A. Rangarajan, and M. H. Yang, "An algebraic approach to affine registration of point sets," in *2009 IEEE 12th International Conference on Computer Vision*, Sept 2009, pp. 1335–1340.

[31] M. Hauglin, J. Dibdiakova, T. Gobakken, and E. Næsset, "Estimating single-tree branch biomass of norway spruce by airborne laser scanning," *{ISPRS} Journal of Photogrammetry and Remote Sensing*, vol. 79, pp. 147 – 156, 2013.

TABLE V: Notation used in this paper reported in apparition order.

Symbol	Description
CHM	(Canopy Height Model) Regularized version of the point cloud converted into an image
$\mathcal{P}_1$, $\mathcal{P}_2$	Point clouds acquired at times t_1 and t_2, respectively, composed by points $\mathbf{p} = (x, y, z)$
t_1, t_2	Dates of acquisition of the two LiDAR data
ω_n	Not considered areas
Ω_l	Large changes
ω_{lp}	Large positive changes
ω_{ln}	Large negative changes
Ω_c	Forest canopy cover
ω_{ng}	Trees with no significant growth
ω_g	Trees with growth
$\{\mathbf{p}_{1,q}, \mathbf{p}_{2,q}\}_{q=1}^{Q}$	Set of Q matched points of point clouds $\mathcal{P}_1$ and $\mathcal{P}_2$
$T = [R\|t]$	Transformation matrix composed by a rotation matrix R and a translation vector t
w_q	Binary value set to 0 to discard a pair of matched points
$\text{CHM}_D(x, y)$	Difference image of the two CHMs
$\text{CHM}_{D,lp}(x, y)$	Large positive changes map
$\text{CHM}_{D,ln}(x, y)$	Large negative changes map
$\text{CHM}_{D,l}(x, y)$	Large changes (both positive and negative) map
$\mathcal{S} = \mathbf{s}_1, \ldots, \mathbf{s}_N$	Set of identified tree-tops where $\mathbf{s}_k = (x_k, y_k)$
$\ell_{k,j}$	2-D line connecting seed $\mathbf{s}_k$ (first phase of the crown delineation) and a neighbour seed $\mathbf{s}_j$
$\Upsilon_{k,j}$	Values of the CHM over the coordinates defined by $\ell_{k,j}$
$R_{1,k}$, $R_{2,k}$	Regions that delineate the crown of tree $\mathbf{s}_k$ at times t_1 and t_2
$C_{1,k}$, $C_{2,k}$	Segmented point clouds representing tree $\mathbf{s}_k$ at times t_1 and t_2
$H_{1,k}$, $H_{2,k}$	Top height of tree $\mathbf{s}_k$ at times t_1 and t_2
$ch_{1,k}$, $ch_{2,k}$	Crown height of tree $\mathbf{s}_k$ at times t_1 and t_2
bh_k	Base height of tree $\mathbf{s}_k$
$cr_{1,k}$, $cr_{2,k}$	Crown radius of tree $\mathbf{s}_k$ at times t_1 and t_2
cc_k	Crown curvature of tree $\mathbf{s}_k$
$E_{1,k}$, $E_{2,k}$	3-D models representing the structure of tree $\mathbf{s}_k$ at times t_1 and t_2
$V(E_{1,k})$, $V(E_{2,k})$	Crown volume of tree $\mathbf{s}_k$ at times t_1 and t_2
dH_k, dV_k	Vertical growth and crown volume growth of tree $\mathbf{s}_k$

[32] A. Ferraz, S. Saatchi, C. Mallet, and V. Meyer, "Lidar detection of individual tree size in tropical forests," *Remote Sensing of Environment*, vol. 183, pp. 318 – 333, 2016.

[33] D. Riaño, E. Chuvieco, S. Condés, J. González-Matesanz, and S. L. Ustin, "Generation of crown bulk density for pinus sylvestris l. from lidar," *Remote Sensing of Environment*, vol. 92, no. 3, pp. 345 – 352, 2004, forest Fire Prevention and Assessment.

[34] M. A. Finney, *FARSITE: Fire area simulator: model development and evaluation*. US Department of Agriculture, Forest Service, Rocky Mountain Research Station Ogden, UT, 2004.

[35] A. Kato, L. M. Moskal, P. Schiess, M. E. Swanson, D. Calhoun, and W. Stuetzle, "Capturing tree crown formation through implicit surface reconstruction using airborne lidar data," *Remote Sensing of Environment*, vol. 113, no. 6, pp. 1148 – 1162, 2009.

[36] C. Stolojescu-Crişan and A. Isar, "Images compressive sensing reconstruction by inpainting," in *2015 International Symposium on Signals, Circuits and Systems (ISSCS)*, July 2015, pp. 1–4.

[37] F. Morsdorf, E. Meier, B. Kötz, K. I. Itten, M. Dobbertin, and B. Allgöwer, "Lidar-based geometric reconstruction of boreal type forest stands at single tree level for forest and wildland fire management," *Remote Sensing of Environment*, vol. 92, no. 3, pp. 353–362, 2004.

[38] Y. Sheng, P. Gong, and G. Biging, "Model-based conifer-crown surface reconstruction from high-resolution aerial images," *Photogrammetric engineering and remote sensing*, vol. 67, no. 8, pp. 957–966, 2001.

[39] C. Paris and L. Bruzzone, "A three-dimensional model-based approach to the estimation of the tree top height by fusing low-density lidar data and very high resolution optical images," *Geoscience and Remote Sensing, IEEE Transactions on*, vol. 53, no. 1, pp. 467–480, Jan 2015.

[40] H. T. Valentine, R. L. Amateis, J. H. Gove, and A. Mäkelä, "Crown-rise and crown-length dynamics: application to loblolly pine," *Forestry: An International Journal of Forest Research*, vol. 86, no. 3, p. 371, 2013.